LETTERS
DOI: 10.1038/s41566-017-0007-1

nature photonics

Single-qubit quantum memory exceeding ten-minute coherence time

Ye Wang[1], Mark Um[1], Junhua Zhang[1], Shuoming An[1], Ming Lyu[1,3], Jing-Ning Zhang[1], L.-M. Duan[1,2], Dahyun Yum[1]* and Kihwan Kim[1]*

A long-time quantum memory capable of storing and measuring quantum information at the single-qubit level is an essential ingredient for practical quantum computation and communication[1,2]. Currently, the coherence time of a single qubit is limited to less than 1 min, as demonstrated in trapped ion systems[3–5], although much longer coherence times have been reported in ensembles of trapped ions[6,7] and nuclear spins of ionized donors[8,9]. Here, we report the observation of a coherence time of over 10 min for a single qubit in a $^{171}Yb^{+}$ ion sympathetically cooled by a $^{138}Ba^{+}$ ion in the same Paul trap, which eliminates the problem of qubit-detection inefficiency from heating of the qubit ion[10,11]. We also apply a few thousand dynamical decoupling pulses to suppress ambient noise from magnetic-field fluctuations and phase noise from the local oscillator[8,9,12–16]. The long-time quantum memory of the single trapped ion qubit would be the essential component of scalable quantum computers[1,17,18], quantum networks[2,19,20] and quantum money[21,22].

The unique quantum-nature-like no-cloning principle, the impossibility of copying quantum information, can be observed and used with only the capability to coherently manipulate and detect an individual quantum system, a qubit in the most elementary level[21,22]. Without accessibility to individual qubits, it is fundamentally inconceivable to store, operate and retrieve quantum information in an ensemble of qubits. It has long been a quest to develop technologies to coherently process and detect quantum information at the single-qubit level. More than twenty years ago, a coherence time of ~10 min was observed in an ensemble of ions with magnetic-field-insensitive states[6,7]. Following more than ten years of developments, the coherence time of a single qubit with magnetic-field-insensitive states was measured[3]. Unexpectedly, the reported coherence time of a single qubit is much shorter than those of ensemble systems. The technology for controlling the field-insensitive qubit has been improved significantly, but the coherence time of a single qubit was still observed to be less than 1 min. Recently, an hour-level coherence time was reported in an ensemble of nuclear spins of ionized donors[8,9], but the coherence time of a single qubit in such solid systems has not yet been reported, to our knowledge.

For trapped ion qubits (in particular, hyperfine qubits), their intrinsic relaxation (with time T_1) is much longer than the dephasing (with time T_2^*) induced by the fluctuation of magnetic fields and the phase noise of the local oscillator in the experiment. The current record for the single-qubit coherence time in trapped ion systems is mainly limited, not by the coherence itself, but by the decreasing state-detection efficiency associated with the motional heating of the ion without laser cooling[10,11]. Due to this motional heating, the wavepacket of the ion expands with time, which reduces the count of fluorescence photons and makes the state discrimination inefficient[10,11]. The motional heating of ions can be significantly suppressed by cleaning the surface of the ion trap[23] or locating the trap in a low-temperature environment[24]. Here, we eliminate the ion heating during long-time storage by sympathetic cooling with a different species of atomic ions.

The long coherence time of a trapped ion qubit is the essential element for practical quantum computation and quantum communication[2,25]. The trapped ion system constitutes one of the leading candidates for the realization of large-scale quantum computers[1]. It also provides a competitive platform for the realization of quantum networks that combines long-distance quantum communication with local quantum computation[2]. One scalable architecture for the ion-trap quantum computer comprises dividing the system into operation and memory zones and connecting them through ion shuttling[17,18]. For this architecture, the basic unit of the operation zone has been demonstrated[26,27]. As the size of the system scales up, the needed storage time of the qubits in the memory zone will correspondingly increase. To keep the qubit error rates below a certain threshold for fault-tolerant computation, it is crucial to extend the coherence time of the qubits. For a quantum network based on probabilistic ion–photon mapping[28], the basic units of ion–photon and ion–ion entanglement have been demonstrated[29–31]. The required coherence time of qubits increases in this approach as the size of the system grows.

For the present experiment we used two species of ion, $^{171}Yb^{+}$ as the qubit ion and $^{138}Ba^{+}$ as the cooling ion, confined together in a standard Paul trap as shown in Fig. 1a. We chose the $^{138}Ba^{+}$ ion as the refrigerator because it has a mass similar to that of $^{171}Yb^{+}$, which makes the sympathetic cooling efficient. The Doppler cooling laser and the repumping laser for $^{138}Ba^{+}$ were detuned by more than 200 THz from the corresponding transitions of the $^{171}Yb^{+}$ ion, so the coherence of the $^{171}Yb^{+}$ qubit was affected negligibly by the cooling laser beam during the Doppler cooling of the $^{138}Ba^{+}$ ion (see Methods). We noticed that the small scattering from the Doppler cooling laser beam for the $^{171}Yb^{+}$ ion introduced serious decoherence, so we developed three cascaded switching methods to completely block the laser beam, as shown in Fig. 1b. The two hyperfine levels of the $^{171}Yb^{+}$ ion in the $^2S_{1/2}$ manifold were used as a qubit represented by $|\downarrow\rangle \equiv |F=0, m_F=0\rangle$ and $|\uparrow\rangle \equiv |F=1, m_F=0\rangle$, separated by $12{,}642{,}812{,}118 + 310.8B^2$ Hz, where B is the magnetic field in gauss (G). In the experiment, we initialized the qubit state to

[1]Center for Quantum Information, Institute for Interdisciplinary Information Sciences, Tsinghua University, Beijing 100084, China. [2]Department of Physics, University of Michigan, Ann Arbor, MI 48109, USA. Present address: [3]Department of Electrical Engineering, Princeton University, Princeton, NJ 08544, USA.
*e-mail: starydh@gmail.com; kimkihwan@mail.tsinghua.edu.cn

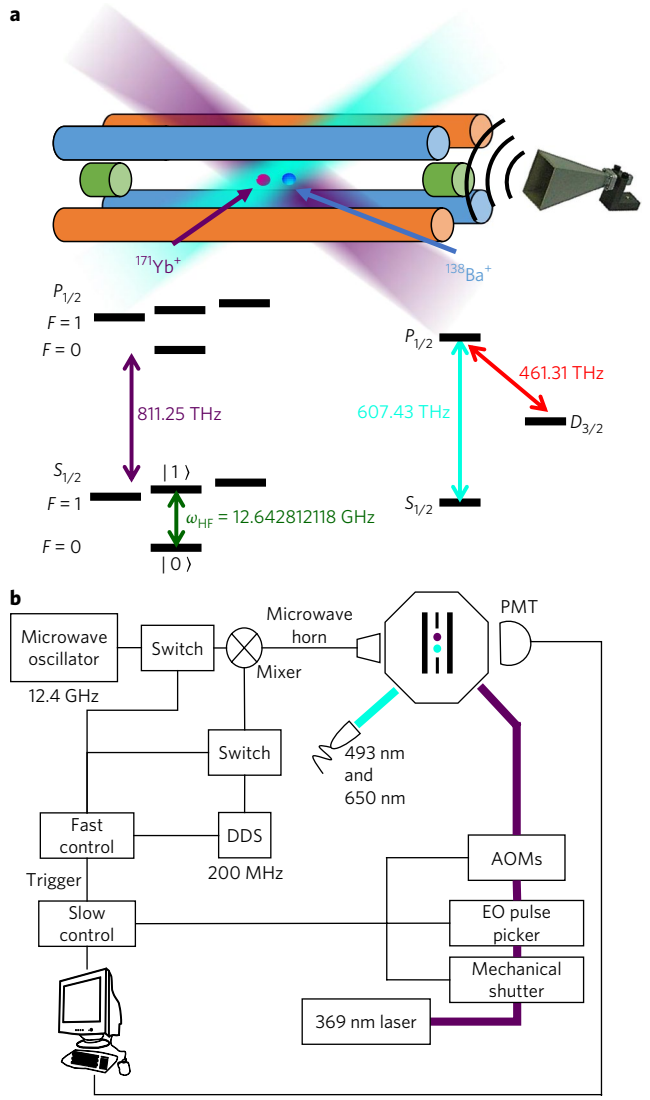

Fig. 1 | Experimental set-up. a, Schematic diagram of a trapped-ion system with two species. We simultaneously trap $^{171}Yb^+$ and $^{138}Ba^+$ ions, separated by a distance of 10 μm, in a linear Paul trap. The laser beams for $^{171}Yb^+$ and $^{138}Ba^+$ cover both ions, so the initialization and detection of $^{171}Yb^+$ is not affected by the change of ion position due to hopping every ~5 min. We do not observe any difference in the strength of the magnetic field and the π time of a single qubit gate for both positions. **b**, Microwave and laser control system. Microwaves are generated by mixing a fixed 12.442812 GHz signal from an Agilent microwave oscillator and the signal around 200 MHz from a direct digital synthesizer (DDS), with the capability of changing phase within 100 ns (controlled by a field-programmable gate array, FPGA). All sources are referenced to a Rb clock. We apply a three-stage switch system for the 369 nm laser beam, consisting of AOMs, an EO pulse picker and a mechanical shutter (see Methods). PMT, photomultiplier tube.

$|\downarrow\rangle$ by the standard optical pumping method and discriminated the state using a florescence detection scheme. We performed coherent manipulation of the qubit by applying a resonant microwave, as shown in Fig. 1b.

With sympathetic cooling, the remaining dominant factors of decoherence are the magnetic field fluctuations and the phase noise of the qubit operational microwave, which leads to phase randomization[13]. We can write the Hamiltonian of the qubit system as $H=\frac{\hbar}{2}(\omega_0+\beta(t))\sigma_z$, where ω_0 is the splitting of the qubit, $\beta(t)=\beta_B(t)+\beta_{LO}(t)$ is the random phase noise that consists of the magnetic field fluctuations β_B and the phase noise β_{LO} of the qubit operational microwave[32], and σ_z is the Pauli operator. The accumulation of the random phase causes dephasing of the qubit state.

A standard technique to preserve the qubit coherence against random phase noise is dynamical decoupling, which consists of multiple spin-echo pulses[8,9,12–16]. Because the performance of the sequence is sensitive to the characteristics of the noise environment, we studied the noise spectrum of our system, which guided us to choose proper dynamical decoupling pulses. In the experiment, we probed the specific frequency part of the noise spectrum by monitoring the response of the qubit under the specific sequence[33]. The initial state of qubit $|\psi(0)\rangle$ under a dynamical decoupling sequence in a noisy environment evolves according to $|\psi(T)\rangle=e^{iF_N(T)\sigma_z}|\psi(0)\rangle$, where $F_N(T)=\sum_{i=0}^{N}(-1)^{i+1}\int_{\tau_i}^{\tau_{i+1}}dt\beta(t)$, T is the total evolution time, and τ_i is the time stamp of the ith π pulse. We obtained the information for $F_N(T)$ by measuring the contrast of the Ramsey fringe as $\langle\cos(2F_N(T))\rangle$, which we define as the coherence of the qubit (see Methods). We then set the magnetic field strength to 8.8 G and applied the CPMG (Carr, Purcell, Meiboom and Gill)[16] sequence shown in Fig. 2a to measure the noise spectrum of the environment.

In our system, the dominant components of noise are at 50 Hz and the harmonics coming from the power line, which is modelled as the sum of discrete noises $\tilde{\beta}(\omega)=\sum_{k=1}^{d}\beta_k\delta(\omega-\omega_k)$. Here, β_k is the strength of the noise. The Ramsey contrast of the final state becomes[14]

$$\langle\cos(2F_N(T))\rangle=\prod_{k=1}^{d}J_0(|\beta_k\tilde{y}(\omega_k,T)|) \quad (1)$$

where J_0 is the 0th Bessel function, $\tilde{y}(\omega,T)=\frac{1}{\omega}\sum_{j=0}^{N}(-1)^j[e^{i\omega\tau_j}-e^{i\omega\tau_{j+1}}]$, $\tau_0=0$, and $\tau_{N+1}=T$. With 31 pulses, we obtain the resultant coherence (as a function of the pulse interval) shown in Fig. 2b. By fitting, we obtain the discrete noise spectrum as $B_{50Hz}=18.3$ μG, $B_{150Hz}=57.5$ μG, with no significant components at other frequencies.

We studied the rest of the noise spectrum by using the continuous noise model. Given an arbitrary noise spectrum $S_\beta(\omega)$, the Ramsey contrast is given by $e^{-\chi(T)}$, where $\chi(T)$ is written as[13]

$$\chi(T)=\frac{2}{\pi}\int_0^\infty S_\beta(\omega)|\tilde{y}(\omega,T)|^2d\omega \quad (2)$$

Here the function $|\tilde{y}(\omega,T)|^2$ can be viewed as a bandpass filter with a centre frequency of $\frac{1}{2\tau}$ and the width proportional to $\frac{1}{2\pi T}$, where τ is the pulses interval shown in Fig. 2a. Figure 2c shows the Ramsey contrasts in dependence on the total evolution time T with various total numbers of pulses N (2, 10, 100, 500, 4,000, 6,000 and 10,000). Applying equation (2) to the results of Fig. 2c, we obtain $S_\beta(\omega)$, as shown in Fig. 2d. We observe a sharp increase in noise strength below (2π) 2 Hz, which is consistent with the results of flux gauge measurements. We also observe a slow increase in the noise above (2π) 100 Hz, which comes from the phase noise of the operational microwave.

To extend the coherence time with the CPMG type of sequence under our current noise environment, we carefully chose the interval of the pulse sequence. We can locate the bandpass frequency between 2 Hz and 100 Hz, where the noise spectrum has its lowest value, which means $5<\tau<250$ ms. In this range, a larger τ is preferred, as this reduces the number of pulses and leads to a smaller accumulation of gate errors. We chose the pulse interval τ properly so that the noise components at 50 Hz and 150 Hz were suppressed to a negligible level. Considering all the factors, the optimal τ was found to be 200 ms.

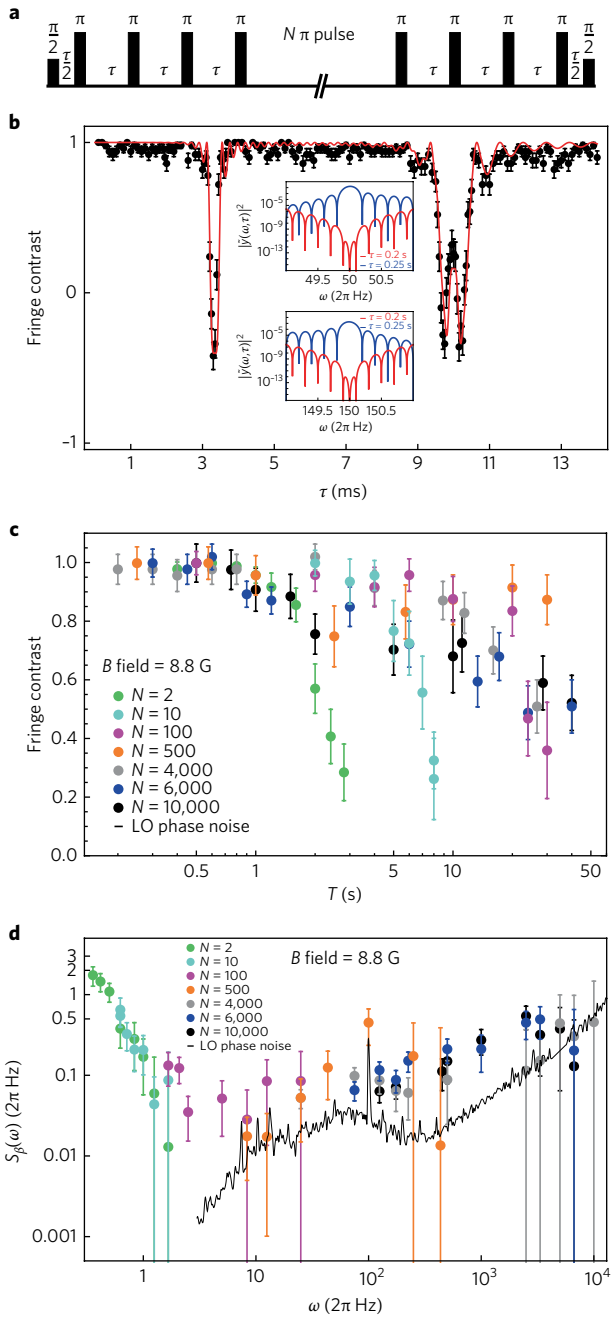

Fig. 2 | Measurement of the noise spectrum of the system. a, Diagram of the CPMG sequence. All the π pulses have the same phase of π/2. Each interval between π pulses is τ. **b**, Fringe contrast $\langle\cos(2F_N(T))\rangle$ as a function of the pulse interval for 31 CPMG pulses. By fitting the data with equation (1), we obtain $B_{50Hz}=18.3\,\mu G$, $B_{150Hz}=57.5\,\mu G$. To suppress 50 Hz and 150 Hz noises with the KDD_{xy}, we chose $\tau=200$ ms instead of 250 ms, because the values of $|\tilde{y}|^2$ near 50 Hz and 150 Hz are around 10 orders of magnitude lower, as shown in the insets. Error bars are the standard deviations of 100 repetitions. **c**, Ramsey contrasts $\langle\cos(2F_N(T))\rangle$ depending on total evolution time for various numbers of pulses ($N=2$, 10, 100, 500, 4,000, 6,000 and 10,000). Data are normalized to the contrast of the data for the same number of pulses without waiting times. Error bars are standard deviations of 50 to 200 repetitions. **d**, Analysed noise spectra from the coherence decay shown in **c**, obtained with equation (2). The smallest noise level is located at the range of (2π) ~2–100 Hz. The black line shows the phase noise for the operational microwave measured by an Agilent PXA spectrum analyser. LO, local oscillator.

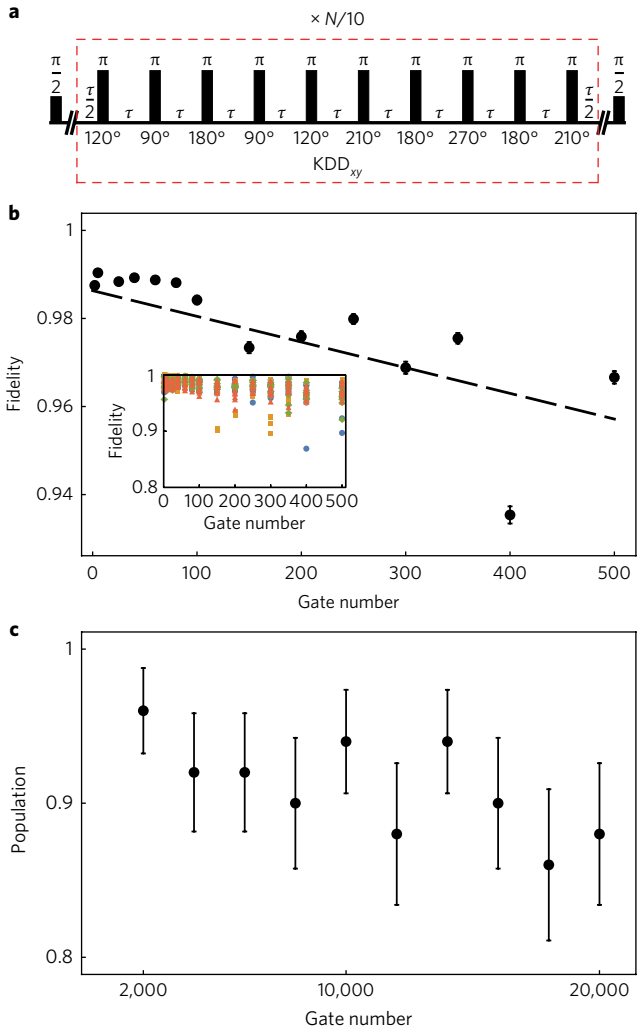

Fig. 3 | KDD_{xy} sequence and gate fidelity. a, Diagram of the KDD_{xy} sequence. The Knill pulse consists of five π pulses with angles $\varphi+\pi/6$, φ, $\varphi+\pi/2$, φ and $\varphi+\pi/6$. The KDD_{xy} consists of two Knill pulses equally spaced with $\varphi=\pi/2$ and $\varphi=\pi$. We apply $N/10$ sets of the KDD_{xy}, which leads to a total of N pulses. Note that N should be a multiple of 20 to form an identity operation[15]. **b**, Randomized benchmarking test of the single qubit gates. We use 32 settings of random sequences (following ref. [34]). Inset: results of 32 different settings. Each data point represents the average of 500 experiments. Black circles in the main graph represent the average values of 32 settings and error bars are standard deviations. By fitting, we obtain the gate fidelity as 99.994 ± 0.002%. **c**, We continuously applied the KDD_{xy} pulses on the initial $|\uparrow\rangle$ state to test its performance. We observe more than 85% of the population revert to the initial $|\uparrow\rangle$ state after application of 20,000 π pulses. Error bars are standard deviations.

In the experiment, we used the KDD_{xy} (Knill dynamical decoupling pulse) (refs [9,15]) sequence to store the arbitrary quantum states of a single qubit. KDD_{xy} is a robust dynamical decoupling sequence insensitive to imperfections in gate operations, including flip-angle errors and off-resonance errors. As shown in Fig. 3a, KDD_{xy} can be considered as an extension of the CPMG sequence (see Methods). Our single qubit gate fidelity was measured to be 99.994 ± 0.002% by a randomized benchmarking method[34] (Fig. 3b). We tested the robustness of the KDD_{xy} by continuously applying it to the $|\uparrow\rangle$ state. After the application of 20,000 pulses, more than 85% of the population had reverted to the initial $|\uparrow\rangle$ state (Fig. 3c).

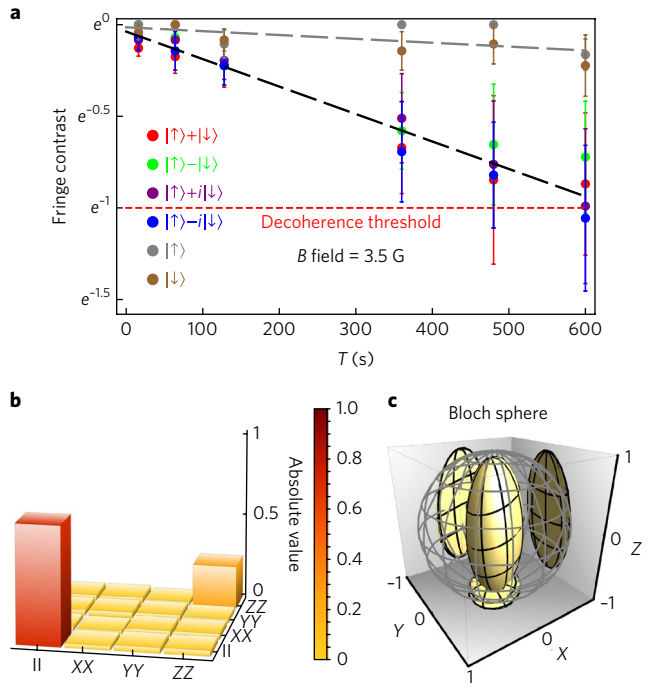

Fig. 4 | Coherence time measurement and quantum process tomography. **a**, Coherence time of six different initial states. For states $|\uparrow\rangle$ and $|\downarrow\rangle$, the coherence time is 4,740 ± 1,760 s, which is obtained by fitting the data points, as shown by the grey dashed line. For the other four initial states, the coherence time is 667 ± 17 s, which is attained by fitting the data points, as shown by the black dashed line. Error bars are standard deviations. **b**, Results of quantum process tomography for a duration of 8 min. Here, the tomography is obtained from the entire process including initialization, storage and detection. Identity is the dominant diagonal part with $\chi_{II} = 0.699 \pm 0.058$. **c**, Transformation from the initial states lying on the meshed surface to the final states lying on the solid surface after 8 min of storage.

For measurement of the single-qubit coherence time, we set the magnetic field to 3.5 G to reduce the influence of magnetic field noise (see Methods). We measured the coherence time of the single-qubit memory with six different initial states: $|\uparrow\rangle, |\downarrow\rangle, 1/\sqrt{2}(|\uparrow\rangle + |\downarrow\rangle)$, $1/\sqrt{2}(|\uparrow\rangle - |\downarrow\rangle), 1/\sqrt{2}(|\uparrow\rangle + i|\downarrow\rangle), 1/\sqrt{2}(|\uparrow\rangle - i|\downarrow\rangle)$. In Fig. 4a, we see no significant relaxation for the initial states of $|\uparrow\rangle$ and $|\downarrow\rangle$ under the KDD_{xy} sequence. The reduction of their contrasts mainly arises from the accumulation of gate errors. The other four initial states have a similar decoherence rate, which corresponds to a coherence time of 667 ± 17 s from exponential decay fitting. The demonstrated coherence time is primarily limited by the non-vanishing noise strength at the bandpass filter frequency of 2.5 Hz. We also performed process tomography on our dynamical decoupling process for 8 min. The results shown in Fig. 4b,c demonstrate that the process is approximated as an identity operator with the main error corresponding to pure dephasing, in agreement with our knowledge about the hyperfine qubit of the trapped-ion system.

We note that our measured coherence time over 10 min is not fundamentally limited. The coherence time can be further increased by decreasing $S_\beta(\omega)$ at the bandpass frequency, which can be achieved by installing a magnetic field shield, using a magnetic-field-insensitive qubit at the zero crossing regime or using a better microwave oscillator. The number of memory qubits can be increased with sympathetic cooling for quantum cryptographic applications including quantum money[21,22]. Our demonstration of long coherence time would stimulate the development of hybrid set-ups that map quantum information in systems with limited quantum memory including superconducting qubits into the trapped ion qubit[35,36].

Methods

Methods, including statements of data availability and any associated accession codes and references, are available in the online version of this paper.

Received: 12 January 2017; Accepted: 4 August 2017;
Published online: 25 September 2017

References

1. Ladd, T. D. et al. Quantum computers. *Nature* **464**, 45–53 (2010).
2. Duan, L.-M. & Monroe, C. Quantum networks with trapped ions. *Rev. Mod. Phys.* **82**, 1209–1224 (2012).
3. Langer, C. et al. Long-lived qubit memory using atomic ions. *Phys. Rev. Lett.* **95**, 060502 (2005).
4. Häffner, H. et al. Robust entanglement. *Appl. Phys. B* **81**, 151–153 (2005).
5. Harty, T. et al. High-fidelity preparation, gates, memory, and readout of a trapped-ion quantum bit. *Phys. Rev. Lett.* **113**, 220501 (2014).
6. Bollinger, J., Heizen, D., Itano, W., Gilbert, S. & Wineland, D. A 303-MHz frequency standard based on trapped Be^+ ions. *IEEE Trans. Instrum. Meas.* **40**, 126–128 (1991).
7. Fisk, P. et al. Very high *Q* microwave spectroscopy on trapped $^{171}Yb^+$ ions: application as a frequency standard. *IEEE Trans. Instrum. Meas.* **44**, 113–116 (1995).
8. Saeedi, K. et al. Room-temperature quantum bit storage exceeding 39 minutes using ionized donors in silicon-28. *Science* **342**, 830–833 (2013).
9. Zhong, M. et al. Optically addressable nuclear spins in a solid with a six-hour coherence time. *Nature* **517**, 177–180 (2015).
10. Epstein, R. J. et al. Simplified motional heating rate measurements of trapped ions. *Phys. Rev. A* **76**, 033411 (2007).
11. Wesenberg, J. et al. Fluorescence during Doppler cooling of a single trapped atom. *Phys. Rev. A* **76**, 053416 (2007).
12. Khodjasteh, K. et al. Designing a practical high-fidelity long-time quantum memory. *Nat. Commun.* **4**, 2045 (2013).
13. Biercuk, M. J. et al. Optimized dynamical decoupling in a model quantum memory. *Nature* **458**, 996–1000 (2009).
14. Kotler, S., Akerman, N., Glickman, Y. & Ozeri, R. Nonlinear single-spin spectrum analyzer. *Phys. Rev. Lett.* **110**, 110503 (2013).
15. Souza, A. M., Álvarez, G. A. & Suter, D. Robust dynamical decoupling for quantum computing and quantum memory. *Phys. Rev. Lett.* **106**, 240501 (2011).
16. Haeberlen, U. *High Resolution NMR in Solids Selective Averaging* (Elsevier, 1976).
17. Kielpinski, D., Monroe, C. & Wineland, D. J. Architecture for a large-scale ion-trap quantum computer. *Nature* **417**, 709–711 (2002).
18. Lekitsch, B. et al. Blueprint for a microwave trapped ion quantum computer. *Sci. Adv.* **3**, e1601540 (2017).
19. Monroe, C. & Kim, J. Scaling the ion trap quantum processor. *Science* **339**, 1164–1169 (2013).
20. Nickerson, N. H., Fitzsimons, J. F. & Benjamin, S. C. Freely scalable quantum technologies using cells of 5-to-50 qubits with very lossy and noisy photonic links. *Phys. Rev. X* **4**, 041041 (2014).
21. Wiesner, S. Conjugate coding. *ACM SIGACT News* **15**, 78–88 (1983).
22. Pastawski, F., Yao, N. Y., Jiang, L., Lukin, M. D. & Cirac, J. I. Unforgeable noise-tolerant quantum tokens. *Proc. Natl Acad. Sci. USA* **109**, 16079–16082 (2012).
23. Hite, D. A. et al. 100-fold reduction of electric-field noise in an ion trap cleaned with in situ argon-ion-beam bombardment. *Phys. Rev. Lett.* **109**, 103001 (2012).
24. Deslauriers, L. et al. Scaling and suppression of anomalous heating in ion traps. *Phys. Rev. Lett.* **97**, 103007 (2006).
25. Nielsen, M. A. & Chuang, I. L. *Quantum Computation and Quantum Information* (Cambridge Univ. Press, 2010).
26. Home, J. P. et al. Complete methods set for scalable ion trap quantum information processing. *Science* **325**, 1227–1230 (2009).
27. Hanneke, D. et al. Realization of a programmable two-qubit quantum processor. *Nat. Phys.* **6**, 13–16 (2010).
28. Duan, L. M., Blinov, B. B., Moehring, D. L. & Monroe, C. Scalable trapped ion quantum computation with a probabilistic ion-photon mapping. *Quantum Inf. Comput.* **4**, 165–173 (2004).

29. Blinov, B., Moehring, D., Duan, L.-M. & Monroe, C. Observation of entanglement between a single trapped atom and a single photon. *Nature* **428**, 153–157 (2004).
30. Moehring, D. L. et al. Entanglement of single atom quantum bits at a distance. *Nature* **449**, 68–71 (2007).
31. Kurz, C. et al. Experimental protocol for high-fidelity heralded photon-to-atom quantum state transfer. *Nat. Commun.* **5**, 5527 (2014).
32. Ball, H., Oliver, W. D. & Biercuk, M. J. The role of master clock stability in quantum information processing. *Nat. Quantum Inf.* **2**, 16033 (2016).
33. Bylander, J. et al. Noise spectroscopy through dynamical decoupling with a superconducting flux qubit. *Nat. Phys.* **7**, 565–570 (2011).
34. Knill, E. et al. Randomized benchmarking of quantum gates. *Phys. Rev. A* **77**, 012307 (2008).
35. Kielpinski, D., Kafri, D., Woolley, M. J., Milburn, G. J. & Taylor, J. M. Quantum interface between an electrical circuit and a single atom. *Phys. Rev. Lett.* **108**, 130504 (2012).
36. Daniilidis, N., Gorman, D. J., Tian, L. & Hffner, H. Quantum information processing with trapped electrons and superconducting electronics. *New J. Phys.* **251**, 073017 (2013).

Acknowledgements

This work was supported by the National Key Research and Development Program of China under grant 2016YFA0301900 (no. 2016YFA0301901) and the National Natural Science Foundation of China grants 11374178, 11504197 and 11574002.

Author contributions

Y.W. and D.Y. developed the experimental system. Y.W., with the participation of M.U. and D.Y., collected and analysed the data. J.Z. and S.A. provided technical support. M.L., J.-N.Z., L.-M.D. and D.Y. provided theoretical support. K.K. supervised the project. All authors contributed to writing the manuscript.

Competing interests

The authors declare no competing financial interests.

Additional information

Reprints and permissions information is available at www.nature.com/reprints.

Correspondence and requests for materials should be addressed to D.Y. or K.K.

Publisher's note: Springer Nature remains neutral with regard to jurisdictional claims in published maps and institutional affiliations.

Methods

Control system. We used two field-programmable gate array (FPGA) boards to separately control the laser system and microwave system. The two parts were synchronized to less than 10 ps of time jitter. Leakage from the 369 nm laser beams greatly limits the coherence time of the qubit of the $^{171}Yb^+$ ion. To block the 369 nm laser beams for Doppler cooling, initializing and detecting the quantum state of the $^{171}Yb^+$ ion, we used three stages of switches: acousto-optic modulators (AOMs), an electro-optic (EO) pulse picker and a mechanical shutter. The AOM switches leave behind a few nanowatts of laser beam leakage, the EO pulse picker provides 200-fold attenuation for the leakage, and the mechanical shutter blocks the laser beam completely with a response time of about 50 ms. With only the AOM switches, we observes a maximum coherence time of 50 ms. The coherence time was increased to 10 s by applying the EO pulse picker and a dynamical decoupling sequence. It was thus necessary to use the mechanical shutter to completely block the laser beam. The resonant microwave (frequency of 12.642812 GHz) was generated by mixing the signal of a microwave oscillator with the signal of around 200 MHz of a direct digital synthesizer (DDS). The DDS was used to change the phase of the microwave within 100 ns, which was controlled by the FPGA. All sources were referenced to a Rb clock.

Limitation of coherence time due to the cooling laser beams for $^{138}Ba^+$. We calculate the scattering rate between the $^2S_{1/2}$ manifold and the $^2P_{1/2}$, $^2P_{3/2}$ manifold of $^{171}Yb^+$ due to the cooling laser beams (493 nm and 650 nm) for the $^{138}Ba^+$ ion. The scattering rate was calculated by the model of Raman scattering and Rayleigh elastic scattering[37–39], which is given as

$$\Gamma_{\mathrm{scat}}=\frac{g^2\Gamma}{6}\left(\frac{1}{\Delta_{\mathrm{D1}}^2}+\frac{2}{(\Delta_{\mathrm{D1}}+\Delta_{\mathrm{fs}})^2}\right) \tag{3}$$

where $\Gamma\approx 2\pi\times 20$ MHz, $g=\frac{\Gamma}{2}\sqrt{\frac{I}{2I_{\mathrm{sat}}}}$ and $\Delta_{\mathrm{fs}}\approx 2\pi\times 100$ THz. For the 493 nm laser, the parameters were as follows: laser power $P=40$ μW, beam waist $\omega=22$ μm, $I_{493}=49.6I_{\mathrm{sat}}$ and $\Delta_{\mathrm{D1}}=203.8$ THz, which yields a scattering rate of 2.37×10^{-6} Hz. For the 650 nm laser, the parameters are as follows: laser power $P=10$ μW, beam waist $\omega=20.7$ μm, $I_{650}=14.0I_{\mathrm{sat}}$ and $\Delta_{\mathrm{D1}}=349.9$ THz, which yields a scattering rate of 2.6×10^{-7} Hz. The 493 nm and 650 nm laser beams thus have no effect on the coherence of the $^{171}Yb^+$ ion hyperfine qubit during hours of storage.

Magnetic field fluctuations. The second-order Zeeman effect of the $^{171}Yb^+$ qubit transition[40] is described by $\Delta f_{2\mathrm{OZ}}=K\langle B^2\rangle$ Hz, $K=310.8\,\mathrm{Hz\,G^{-2}}$. In the Hamiltonian $H=\frac{\hbar}{2}\left(\omega_0+\beta_{\mathrm{B}}(t)+\beta_{\mathrm{LO}}(t)\right)\sigma_z$, where ω_0 and $\beta_B(t)$ are given by

$$\omega_0=\omega_{\mathrm{HF}}+K\left(B_x^2+B_y^2+B_z^2\right) \tag{4}$$

$$\beta_B(t)=K(2B_x\langle b_x(t)\rangle+2B_y\langle b_y(t)\rangle+2B_z\langle b_z(t)\rangle+\langle b_x(t)^2\rangle+\langle b_y(t)^2\rangle+\langle b_z(t)^2\rangle) \tag{5}$$

and ω_{HF} is the hyperfine splitting, B_x, B_y, B_z represent the average values of the magnetic field in three directions and $b_x(t)$, $b_y(t)$, $b_z(t)$ describe fluctuations in the corresponding directions. The fluctuations come mainly from the surrounding electronics and environment, and not much from the current sources generating the magnetic field. We can therefore simply assume that the reducing average magnetic field B does not increase the fluctuations $b_x(t)$, $b_y(t)$ and $b_z(t)$. Thus we can use smaller B to obtain smaller $\beta(t)$, thereby achieving a longer coherence time. Because $b_x(t)$ is much smaller than $b_y(t)$ and $b_z(t)$ according to flux gauge measurements, we located the magnetic field along the x axis. In the experiment, we set $B_z=0$, $B_y=0$ and $B_x=3.5$ G, which is the smallest magnetic field strength to maintain detection efficiency in our system. To study the noise spectrum of our system, we used $B_z=0$, $B_y=0$ and $B_x=8.8$ G.

Dynamical decoupling. In the experiment, CPMG was used to study the noise environment and KDD_{xy} for storage. Here we show that the filter function of KDD_{xy} is the same as that of CPMG. Because all the rotation axes we use are in the x–y plane, we write the rotation as

$$\begin{aligned}D_\phi(\gamma)&=D_z(\phi)D_x(\gamma)D_z(-\phi)\\&=e^{-\frac{i}{2}\sigma_z\phi}e^{-\frac{i}{2}\sigma_x\gamma}e^{\frac{i}{2}\sigma_z\phi}\end{aligned} \tag{6}$$

where φ is the angle between the rotation axis and the x axis, and γ is the rotation angle along the axis. In dynamical decoupling sequences, γ is always π, so $D_x(\pi)=\cos(\pi/2)+i\sigma_x\sin(\pi/2)=i\sigma_x$. In the following we will only use σ_x because the factor i is an irrelevant global phase.

We start from initial state $|\psi(0)\rangle=(|\downarrow\rangle+i\,|\uparrow\rangle)/\sqrt{2}$, and the final state is shown as

$$|\psi(T)\rangle=\widetilde{R}(T)|\psi(0)\rangle \tag{7}$$

$$\widetilde{R}(T)=e^{-i\sigma_z\int_{\tau_N}^{\tau_{N+1}}\beta(t)\mathrm{d}t}D_{\phi_N}(\pi)\cdots D_{\phi_2}(\pi)e^{-i\sigma_z\int_{\tau_1}^{\tau_2}\beta(t)\mathrm{d}t}D_{\phi_1}(\pi)e^{-i\sigma_z\int_{\tau_0}^{\tau_1}\beta(t)\mathrm{d}t} \tag{8}$$

where $\widetilde{R}(T)$ is the evolution during total time T, N is the total number of π pulses, τ_i is the time stamp of the ith π pulse, $\tau_0=0$, $\tau_{n+1}=T$ and φ_i is the phase of the ith π pulse. Because N is even for our dynamical decoupling sequence and only σ_x operations in $\widetilde{R}(T)$ flip the spin, we can obtain

$$\widetilde{R}(T)=e^{iF_N(T)\sigma_z} \tag{9}$$

where $F_N(T)$ is a phase term that is obtained by expanding $D_\varphi(\pi)$ in equation (8) with equation (6) as

$$F_N(T)=\sum_{i=0}^{N}(-1)^{i+1}\int_{\tau_i}^{\tau_{i+1}}\beta(t)+\sum_{i=1}^{N}(-1)^{i+1}\phi_i \tag{10}$$

According to equation (9), the Ramsey fringe contrast we measure is[41]

$$\begin{aligned}\langle\psi(T)\,|\,\sigma_y\,|\,\psi(T)\rangle&=\langle\psi(0)|\,\widetilde{R}(T)^\dagger\sigma_y\widetilde{R}(T)\,|\,\psi(0)\rangle\\&=\langle\cos(2F_N(T))\rangle\end{aligned} \tag{11}$$

For normal dynamical decoupling sequences, like CPMG, XY-16 and KDD_{xy}, we have $\sum_{i=1}^{N}(-1)^{i+1}\phi_i=k\pi$, where k is an integer. For KDD_{xy} in particular, N is a multiple of 20 and φ_i cycles in the order $\pi/6$, 0, $\pi/2$, 0, $\pi/6$, $2\pi/3$, $\pi/2$, π, $\pi/2$ and $2\pi/3$. So $\sum_{i=1}^{20}(-1)^{i+1}\phi_i=-\pi$, which means $\langle\cos(2F_N(T))\rangle$ is not affected by $\sum_{i=1}^{N}(-1)^{i+1}\phi_i$. So KDD_{xy} and CPMG with the same interval and pulse number have the same evolution. We can simplify $\langle\cos(2F_N(T))\rangle$ with a discrete and continuous model according to refs [13,14].

Data availability. The data that support the plots within this paper and other findings of this study are available from the corresponding authors upon reasonable request.

References

37. Ozeri, R. et al. Hyperfine coherence in the presence of spontaneous photon scattering. *Phys. Rev. Lett.* **95**, 030403 (2005).
38. Uys, H. et al. Decoherence due to elastic Rayleigh scattering. *Phys. Rev. Lett.* **105**, 200401 (2010).
39. Campbell, W. et al. Ultrafast gates for single atomic qubits. *Phys. Rev. Lett.* **105**, 090502 (2010).
40. Fisk, P. T., Sellars, M. J., Lawn, M. A. & Coles, G. Accurate measurement of the 12.6 GHz clock transition in trapped $^{171}Yb^+$ ions. *IEEE Trans. Ultrason. Ferroelectr. Freq. Control* **44**, 344–354 (1997).
41. Uhrig, G. S. Exact results on dynamical decoupling by π pulses in quantum information processes. *New J. Phys.* **10**, 083024 (2008).